

A

The Spacecraft Structure and Thermal Design Considerations

By P. HRYCAK, D. E. KOONTZ, G. MACCS, I. W. STAFFORD,
B. A. UNGER, and A. M. WITTENBERG

(Manuscript received March 22, 1963)

10877

This paper covers the general structural and thermal design considerations of the Telstar satellite. The basic objectives were to maintain the electronic components in a near room temperature environment and to protect the electronics package from high-frequency vibration excitation. These objectives were realized by dividing the satellite into two lumped masses, the shell and the centrally located electronics package, and by utilizing nylon lacing for support of the electronics package. The package was provided with an active temperature control, regulating radiative heat flow between the skin and the package. Results of on-the-ground experimental evaluation and of telemetry data are given.

R 0740 R

I. INTRODUCTION

The general size and shape constraints for the Telstar satellite have been reviewed in a previous paper.¹ The present paper discusses the important features of the spacecraft structural and thermal design.

The function of the spacecraft structure is to support and isolate the electronic components from the shock and vibration loads due to launch, and to provide a geometry compatible with an isotropic solar cell power plant.²

Since a majority of the critical components used in the electronics package were designed to operate in a room temperature environment, a major objective of the thermal design was to provide a package temperature as close to room temperature as possible. This objective was to be maintained during a two-year life in orbit. Therefore, all orbital effects on the satellite temperature had to be considered: full sunlight, maximum eclipse orbit, seasonal variation of the solar constant, satellite orientation, and long-term effects on surface coatings exposed to ultraviolet light and other radiation effects. Another thermal objective

973

In its Telstar 1,
p 975-1005 refs

Vol. 1 Jun. 1963
(See N64-10868 02-01)

was that the solar cell power plant operate at as low a temperature as practicable, for maximum efficiency in the conversion of solar energy to electrical power.

These apparently contradictory objectives — warm package and cold skin — were met by compacting the electronics components in a central container referred to as the “electronics package,” isolating them from conductive heat transfer to the skin, and providing an active temperature control which regulates the radiant heat transfer from the electronics package to the colder skin. The power from the solar plant, which is dissipated in the electronics package, provides the heat to keep the electronics near room temperature.

The over-all design concept of the Telstar spacecraft structure is depicted in Fig. 1. A “ball-within-a-ball” configuration is employed. Those portions of the outer shell not used for supporting the solar cell power plant are coated with plasma-sprayed aluminum oxide, to keep the satellite skin temperature at about 30°F for best efficiency of the solar cell power plant. The inner “ball” contains the electronics circuitry, which is hermetically sealed from the high vacuum of space. The nylon lacing minimizes thermal conduction from the warm package to the colder skin. To minimize temperature effects on the chassis when

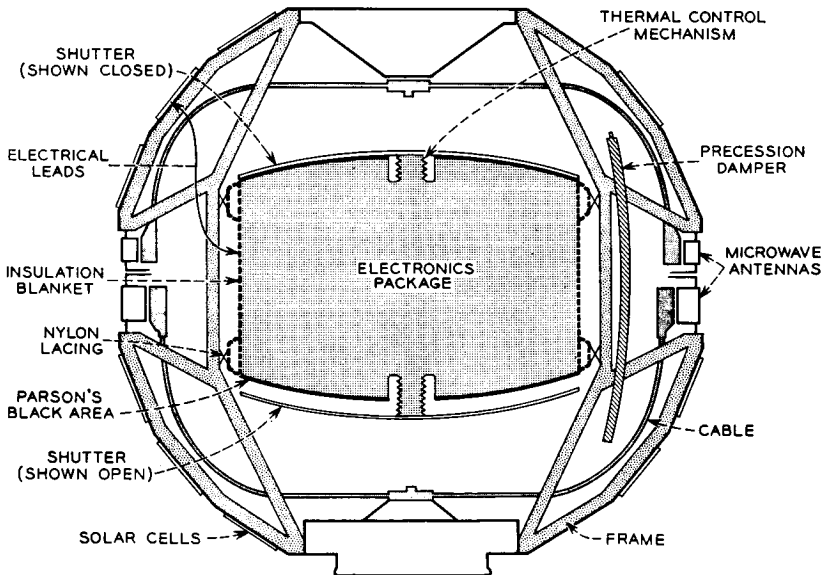


Fig. 1 — Sectional schematic of spacecraft.

the satellite is in either a fully sunlit orbital period or a maximum eclipse period, the radiative heat transfer between the insulated package and the satellite skin is varied by means of thermally actuated shutters. Fig. 2 shows the internal arrangement of the spacecraft parts.

The significant feature of the compact electronics package is that the critical components can be housed in a separate container and through suitable suspension be protected from the high-frequency vibration excitation due to launch. It seemed prudent to protect the electronics from high-frequency vibration excitation, since vibrational failure of electronic devices is most likely to occur in this frequency range. Nylon lacing which supports the electronics package provides both the high-frequency vibration and thermal conductive isolation. This arrangement required that the spacecraft structure support a lumped mass of about 85 pounds subjected to combined vibration and rocket thrust loading. During resonance of the electronics package in its nylon lacing support, the frame must support a combined loading of about 6000 pounds in the thrust direction.

The Telstar satellite is spin stabilized. In a geomagnetic field, its spin rate will be slowed down by induced eddy currents. For this reason, the

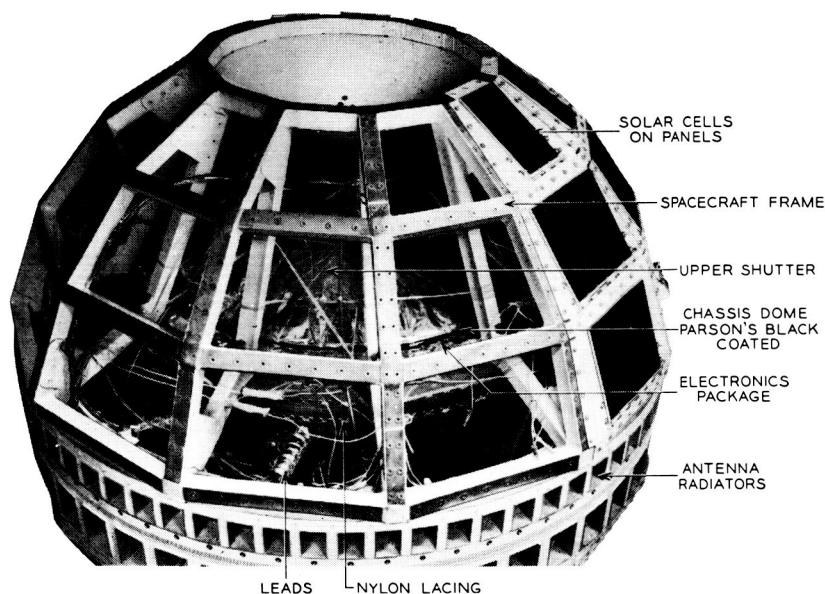


Fig. 2 — Side view of electronics package in spacecraft, showing upper shutter open.

shell is divided into two hemispheres, which are electrically insulated from each other.

Precession dampers are required to keep the satellite spinning about its principal axis of maximum moment of inertia, which is also the symmetry axis of the antenna. Disturbances which could cause a spinning satellite to have short-time precession (wobble) are electromagnetic torques, the uneven forces imparted by the spring during separation from the rocket, and collisions with meteoroids. Precession dampers quickly remove this wobble.³

II. SPACECRAFT CONSTRUCTION AND DESIGN

2.1 *Frame Construction and Design*

The frame of the Telstar satellite is the basic load carrying structure. It must support all other components, and it comprises 13 per cent of the total spacecraft weight of about 170 pounds. The frame provides support for the skin, which is roughly spherical in shape and has a nominal diameter of 34.5 inches. The frame is of an all-welded construction, fabricated from $\frac{3}{4}$ -inch square ZK-21-A magnesium alloy tubing with a wall thickness of 0.025 inch. The frame is constructed in two parts, as shown in Fig. 3.

The sections of the frame are made of 12 truss assemblies, 30 degrees apart; the assemblies are joined by chordal members at their exterior

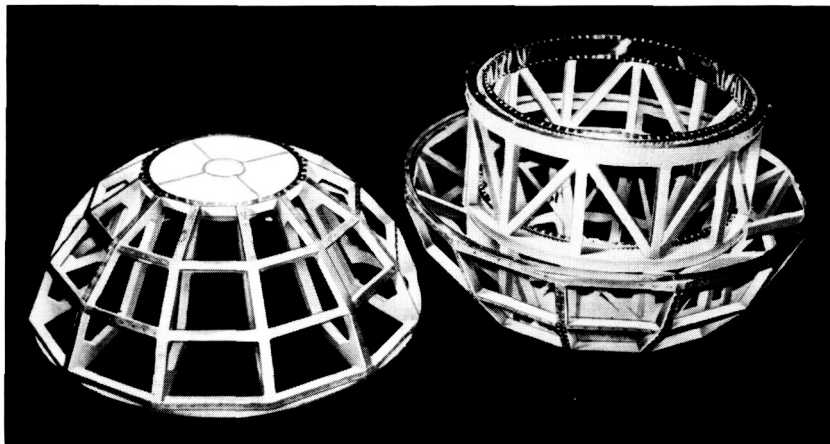


Fig. 3 — Spacecraft frame: upper half at left, lower half at right.

joints. The size of the facets, which is determined by the spacing of the truss assemblies, was selected to provide mounting surfaces of sufficient size for the solar cell modules.² One-half of the framework contains additional structural members, which form a cylindrical cage to support the 85-pound electronics package. The end rings of this cage are made from AZ-31-B-H24 magnesium alloy and contain radial holes with eyelet inserts for lacing the electronics package mounting rings to the frame. A machined AZ-31-B-H24 magnesium alloy plate, which is used to attach the spacecraft to the launch vehicle, is welded to this portion of the frame. In addition, several diagonal members are incorporated into this part of the framework to provide torsional and lateral rigidity.

Because of the mass of the electronics package, the combined sustained acceleration loading due to the thrust of the launch vehicle and the vibrational loading due to the first resonance of the electronics package had to be given special consideration in the frame design. The average (mean) stress in the frame members was limited to a value below the minimum guaranteed compressive yield stress of the ZK-21-A magnesium alloy tubing. The mean stress figure included an appropriate weld efficiency factor, which was determined experimentally. Sufficient rigidity was provided in the construction to minimize secondary bending stresses in the frame members. Limiting the average stresses in the frame members to values below the compressive yield stress of the ZK-21-A tubing and minimizing secondary bending stresses precluded any possibility of a frame collapse due to the combined loading. For the spacecraft, the allowable buckling stress for the frame members exceeded the compressive yield stress for the ZK-21-A tubing.

The hemispherical portions of the frame are electrically insulated from each other to limit the eddy current paths of the satellite. The frame halves are connected by insulated steel bolts, the only structural connection between the two portions of the frame. The 6-kilomegacycle antenna is supported by the upper half of the framework, and the 4-kilomegacycle antenna by the lower half of the framework. Except for internal wiring, these two antennas are de-insulated from each other.⁴

The faceted surfaces formed by the truss and chordal members support the panels which form the skin on which the solar cell modules are mounted. The solar cell modules which compose the solar power plant are attached to these panels by beryllium copper tabs pulled through mounting slots in the panels and twisted to provide intimate contact of the modules to the panels.² The solar cell panels are attached to the frame by screws held in place by lockwashers.

2.2 Solar Cell Panel Construction and Design

Design objectives for the panels which support the solar cell modules were: (a) minimum weight consistent with structural rigidity requirements, (b) flat exterior panel surface to provide good contact with solar cell modules, and (c) thermal behavior of panels equivalent to that of thin, uniform sheets.

The panels, shown in Figs. 4 and 5, are of an integrally stiffened design. They are of brazed construction, fabricated from 6061-T6 aluminum alloy. Total weight of the panels, excluding modules, is 4 per cent of the satellite weight. The panels essentially consist of a cover sheet with so-called "hat" sections brazed on the inside face (i.e., face interior to the spacecraft) of the cover sheet. The hat sections have large holes which provide for radiant heat transfer by eliminating the effect of the additional reflective surface of the hat section. The brazed construction provides good thermal conduction throughout the panel.

The fundamental frequency of the solar cell panels with modules attached occurs at approximately 200 cps when the panels are screwed to the spacecraft frame. The panel design was a compromise between weight and fundamental frequency. From a structural standpoint, it would have been desirable to design for a resonant frequency above 2000 cps; however, the weight penalty would have been enormous even

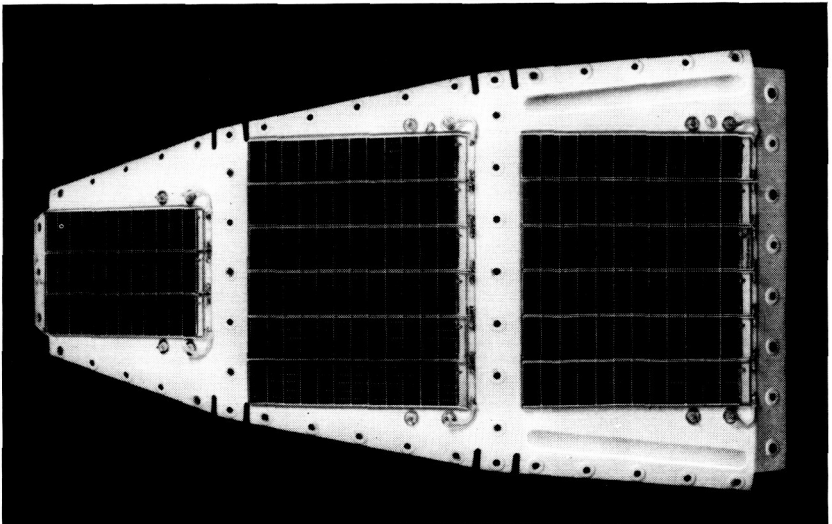


Fig. 4 — Front view of complete solar cell panel.

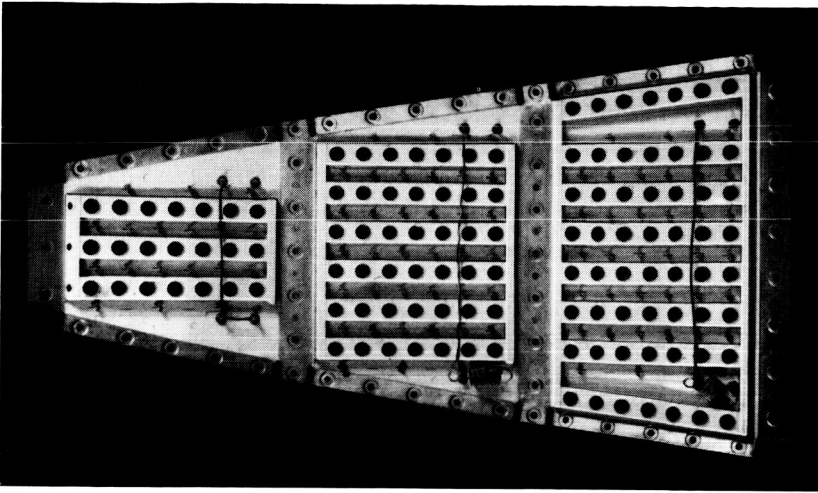


Fig. 5 — Rear view of solar cell panels, showing hat sections.

if such a design could have been achieved. The 200-cps resonance was selected to provide a minimum-weight design which also minimizes deflections of the panel during vibration to avoid damaging the solar cell modules.

Magnesium had been considered for the solar cell supporting panels, with the objective of achieving minimum weight. However, satisfactory brazing techniques were not available for magnesium, and welded construction would have been required. This in turn would have required thicker sections, and the magnesium panel would have weighed about 50 per cent more than the aluminum panel adopted.

2.3 Insulation Support for the Electronics Package

As mentioned previously, the electronics package is supported by nylon lacing to isolate the package from the high-frequency vibrations of launch and, for thermal reasons, to minimize conductive heat transfer to the skin. The spacecraft qualification test specification⁵ suggests the desirability of placing the fundamental resonance of the electronics package below 50 cps; below this frequency, the g level applied to the base of the satellite is minimum (i.e., 0-to-2.3 g peak).

Braided nylon cord was selected for the electronics package lacing because its spring constant would place the fundamental frequency of the electronics package at approximately 42 cps, and yet would have

sufficient strength to support the package under combined loading due to sustained acceleration plus first resonance of the electronics package. Fig. 6 shows that the first resonance of the electronics package occurs at 40 cps; above 40 cps the package is essentially vibrationally isolated from the frame. A similar situation exists for the lateral direction, where the first resonance occurs at 15 cps. Techniques utilizing small spring balances were developed to control the pretensioning of the lacing; as a result, the fundamental frequency of the package was found to be reproducible within a few cps.

In addition to isolating the electronics package from high-frequency vibration, the lacing also supports the package under combined loading and behaves approximately as though it were a linear spring. In the direction of the thrust axis under combined loading, the nylon lacing must withstand a 4050-pound load. Individual braided nylon cord strands are subjected to a load of 32 pounds, which is well below the knot breaking strength of 60 pounds.

Extensive testing of nylon, Dacron, and fiber glass cords was performed to determine their structural characteristics in order to select the appropriate fiber cord with which to lace the electronics package. Load-deflection curves, ultimate strength (unknotted), knot breaking strength, and creep data were obtained for all fibers. The fiber glass cord was rejected for use because of its poor dynamic strength properties. In addition to other tests, the Dacron and nylon cords were subjected to temperature, humidity, high vacuum, and proton and electron radiation

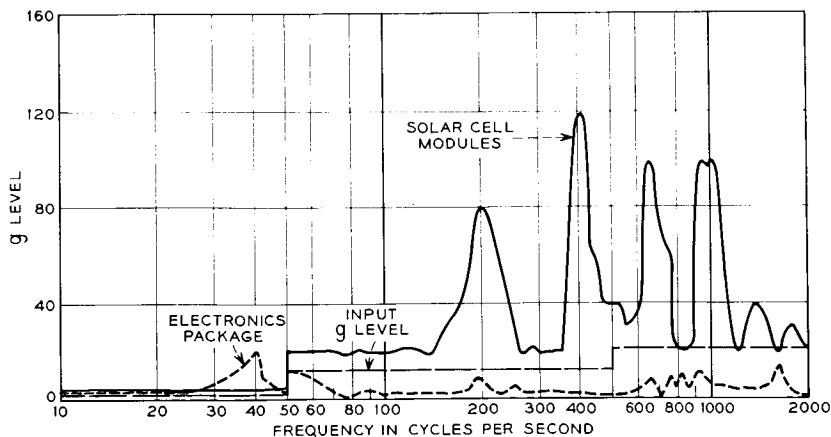


Fig. 6 — Response of electronics package and solar cell modules to sinusoidal vibration excitation in the thrust direction.

tests equivalent to two years in space. Although these tests indicated that there should be no problem with the nylon cord in high vacuum for the desired life of two years, reliability considerations dictated that several pieces of Dacron cord, which is a good deal more space stable than nylon, should also be used to completely insure support of the electronics package.

2.4 Structural Design Testing

The objective of the structural design testing program is to ensure that the complete spacecraft will meet the requirements of the qualification level tests.⁵ It should be noted that the qualification level testing does not include the combined effects of sustained acceleration loading due to the thrust of the launch vehicle and vibrational loading due to the first resonance of the electronics package. Nevertheless, combined loading effects were simulated on an early test model. To meet these objectives, an extensive mechanical test program was instituted in August, 1961, to ensure that (a) the frame structure was capable of withstanding qualification level tests and combined loading, (b) the electronics package was protected from high level vibration excitation during launch, and (c) the spacecraft structure responses during vibration testing were known. The last item determines the appropriate testing levels which should be assigned to the parts connected directly to the satellite frame. Some of these parts are (a) solar cell modules, (b) precession dampers, (c) antenna feed structure, and (d) radiation experiments.

During this extensive structural evaluation program, two vibration test model spacecraft, a structural frame model and a mechanical development model, were used. In October, 1961, the first full-size test model was subjected to shock, centrifuge, and vibration qualification level tests. This model successfully passed the tests and provided the vibration spectrum that the spacecraft components associated with the shell would have to sustain. It also demonstrated that the nylon lacing performed its function of substantially isolating the electronics package from high-frequency vibration excitation. It should be observed that this frame withstood many hours of vibration testing at qualification level, in contrast to the few minutes encountered during launch.

Fig. 6 shows the vibration response of the electronics package and solar cell modules. The required input level to the spacecraft is shown by the heavy dashed line. The design objective of protecting the electronics components from high frequency levels has been substantially achieved. The 20-g level at one discrete frequency at approximately 40 cps is not

undesirable, because electronic components do not have resonances at such a low value. The solar cell modules are subjected to levels as high as 80 to 120 g at several narrow-frequency bands. Amplification factors of 5:1 to 10:1 result from frame resonances, and are to be expected in a structure which is as large as 3 feet in diameter. During resonance dwell tests, which are conducted at the third-stage rocket resonances of 550 to 650 cps, the solar cell modules reached levels as high as 200 g with a 42-g input to the base of the spacecraft.

Another series of vibration tests was performed, using a second vibration test model as a vehicle for the design testing of components which are attached to the frame. Many tests were conducted on the antenna feed structure and techniques were developed for securing their cables.⁴ Tests were also performed to develop the best techniques for securing the many leads and cables connected between the electronics package and frame components. The leads are about 9 inches long, to minimize thermal conduction from the package to the skin.

As mentioned previously, qualification level tests in themselves do not supply absolute proof of the adequacy of the frame and lacing under possible combinations of sustained acceleration and vibration loading due to the first resonance of the electronics package. Static simulation of the possible modes of combined loading were performed on one of the first frames at Lehigh University, Bethlehem, Pennsylvania. The test setup is shown in Fig. 7. All loads were applied to a canister whose outline was similar to that of the electronics package. The canister was specially designed so that the vertical, lateral and torsional loads could be applied to the frame. The method of load application was a conservative approximation to the actual case. The three basic loading conditions, which were applied individually and in suitable combinations, are given in the Table I.

The deflection of the dummy electronics package was measured and strain gauge readings of the various frame members taken. The recorded strains and the stresses calculated therefrom show that the basic spacecraft frame has a margin of safety of 46 per cent for the static loads applied, where due consideration of weld efficiency has been taken into account. The actual margin of safety is somewhat less than 46 per cent, because the static test performed does not completely simulate the fatigue effects of combined vibration and thrust loading. With the present state of the art, this type of test is not possible. Nevertheless, the extensive vibration tests which were conducted on the other models, coupled with the static test, left little room for doubt that the frame is capable of withstanding the actual launch conditions.

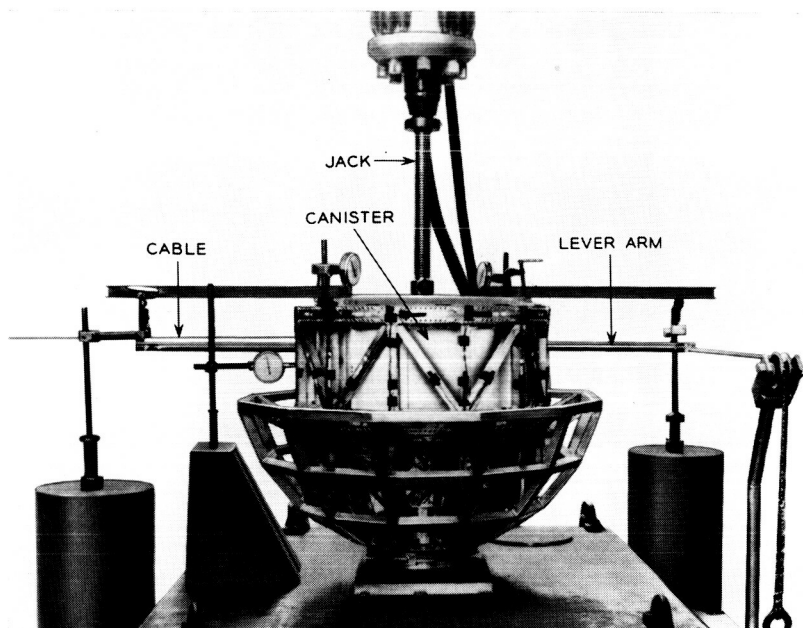


Fig. 7 — Spacecraft static test setup.

TABLE I

Direction of Loading	Due to Sustained Acceleration of 170-lb Satellite	Due to First Resonance of 90-lb Electronics Package	Total Maximum Load
Thrust axis	(25 g) (170 lb) = 4250 lb	(20 g) (90 lb) = 1800 lb	(4250 lb + 1800 lb) = 6050 lb
Transverse (lat- eral) axis	(2.25 g) (170 lb) = 382 lb	(6 g) (90 lb) = 540 lb	(382 lb + 540 lb) = 922 lb
Direction of Loading		Maximum Torque due to Spin-Up	Residual Torque at End of Spin-Up
Torsional moment about spin axis due to flexibility of electronics package mounting		3000 in-lbs	1500 in-lbs

Note: In the thrust direction, the 25-g sustained acceleration is from the rocket thrust and the 20-g vibration acceleration is the level imparted to the package during its resonance. In the transverse direction, the accelerations were determined on a similar basis.

The apparent weight of the satellite along the thrust axis in the 550 to 650-cps frequency range was determined so as to establish the necessary vibration level to be applied in the simulation of the combustion resonance dwell test.⁵ Since the apparent spacecraft weight was of the order of 7 pounds, the combustion test should have been conducted at an 86-g input level over the 550- to 650-cps band. However, vibration equipment was not available to conduct the tests at this high level. Development model spacecraft were tested at a 75-g input level over the required frequency band. As a result of these high-level tests, minor modifications were made to the method of attaching the solar cell modules to the panels and to the interconnections between them. These tests also reconfirmed the adequacy of the spacecraft frame and were useful in proving in many of the components attached to the spacecraft shell structure. Details on qualification tests on the final model are given in Ref. 5.

In December, 1961, a mechanical development model spacecraft, complete except for the electronics package, was subjected to all mechanical tests at qualification level. A dummy weighted canister was used instead of the actual electronics package. This model successfully passed all development tests without failure. In subsequent testing, this model was subjected to the equivalent of four complete qualification-level vibration tests without any failure of any component part.

III. THERMAL DESIGN OF THE SPACECRAFT*

3.1 *Requirements and Design Approach*

The introductory section of this paper outlined the two major thermal design objectives for the Telstar satellite: to provide an environment for the electronics components as close to 70°F as possible, and to maintain the solar cell power plant at as low a temperature as practical. This section of the paper covers the spacecraft thermal design in greater detail.

The temperature of the electronics package shell is used as a reference point to describe the environment for the electronic components. This reference point, of course, is not at the actual temperature of the components themselves. In the design of the electronics package, high-conduction paths were provided to minimize temperature differentials between the components and the package wall. Detailed studies of operating tem-

* Two comprehensive reports on the Telstar satellite thermal design and analysis, including the results of space simulation tests, were submitted to NASA in March and May, 1962. Substantially all of the thermal information reported upon in this paper was included in the foregoing reports.

peratures of internal components provided temperature limits of 15°F to 90°F on the package wall to assure satisfactory operation of the electronics circuitry.¹ Nevertheless, a 70°F objective for the package wall temperature was established, since practically all component life test data were obtained at room temperature.

A knowledge of the temperature distribution over the surface of the satellite was required to determine the power available from the solar cell plant and to establish temperature extremes to which the components attached to the skin would be subjected. These temperature ranges had to be determined in relation to the extremes of the satellite thermal environment.

The thermal and long-life requirements made a good portion of the practical experience gained with other artificial satellites not directly applicable to the Telstar satellite,⁶ and new concepts in the over-all thermal design had to be explored. In particular, thermal analysis disclosed that an active temperature control system was required to minimize temperature variations in the electronics package during a long lifetime in orbit. The control system chosen was unique in that it regulated only the radiative coupling between the package and the skin, while the temperature of the skin itself was to be controlled by passive means. In the early development stages, very little was known of this type of temperature control. Instead, detailed information on an active skin-temperature control, as originally proposed by Hanel⁷ or by Acker,⁸ was available.

3.2 Thermal Radiation Environment of the Telstar Satellite

There are two kinds of thermal radiation which affect Telstar's thermal design: the primary radiation coming directly from the sun and the secondary radiation. Secondary radiation intercepted by the satellite consists of albedo radiation and the earth's infrared radiation. Albedo is solar radiation reflected by the earth. Since energy can be gained or lost in the space environment only by radiation, the extremes of the total radiative heat input had to be determined as the starting point of the entire thermal design.

Direct solar radiation is the major contributor of incident energy, amounting to about 84 per cent of the energy received by the satellite when it is in a fully sunlit orbit. However, this energy may be reduced significantly when the satellite is in an eclipsed orbit. During a maximum 45-minute eclipse in the satellite orbit, the orbital average primary energy will be reduced to 70 per cent of its full sunlit value. In addition,

the direct solar radiation, which may be expressed in terms of the solar constant S , varies ± 3.3 per cent in the course of one year.

The significance of the reflected radiation would, in general, depend on the orientation of the satellite; only in the case of a spherical satellite with an isotropic surface are the effects of the orientation eliminated. Geometrically, the spacecraft was considered to be a sufficiently close approximation to a sphere with an isotropic surface. In addition, the reflected radiation would depend on the altitude of the satellite and its phase angle, defined as the angle between the line joining the sun and the center of the earth and that between the satellite and the earth's center. For a general elliptical orbit, both the altitude and the phase angle will vary with time. The situation is somewhat simpler with regard to the infrared radiation of the earth, which is to a first approximation dependent on the altitude only. The further details of the secondary radiation problem in its relation to spherical satellites have been outlined in a special study.⁹

3.3 *Thermal Model of Telstar Spacecraft and Its Environment*

In the following, as a thermal model, the satellite will be considered to consist of two lumped masses: M_S , with thermal capacitance C_S , corresponding to the skin; and M_P , with thermal capacitance C_P , corresponding to the electronics package of the satellite. Since the package is thermally insulated from the skin by means of a high conductive resistance, all heat transfer between M_S and M_P will have to take place by radiation. Then the package will be, in the steady state, essentially in radiative equilibrium with the skin. In particular, if the time constant of the package is long with respect to the orbital period, a sufficiently close approximation to the steady-state heat transfer will be realized at all times. In other words, the package will then be only very little thermally disturbed by short-term temperature fluctuations of the skin caused by an individual eclipse of the satellite, but will have to adapt itself to long-term orbital changes, i.e., drastic variations of the eclipse periods and seasonal variation in the solar constant.

The long time constant of the package is realized by its high heat capacity and by the application of a low-emissivity material over its surface. The use of the linear concept of a time constant with respect to the relations involving the fourth-power law of radiation is only a convenient approximation.

For a sufficiently uniform temperature prevailing within the package, the temperature extremes of the package will be based on the extremes of the heat radiation intercepted by the skin. This dependence may be

expressed in terms of a reference skin temperature, as discussed in Section 3.4. An expression for such a reference skin temperature, \bar{T}_s , is given by

$$T_s = \left(\frac{S}{4\sigma}\right)^{\frac{1}{4}} \left[\frac{\bar{\alpha}}{\bar{\epsilon}} \left(1 - \frac{t_e}{t_o} + \bar{\alpha}\bar{f}\right) + \frac{1}{4} (1 - \bar{\alpha})\bar{g} \right]^{\frac{1}{4}} \quad (1)$$

where S is the solar constant, σ the Stefan-Boltzmann constant, $\bar{\alpha}$ the over-all value of solar absorptivity of the skin of the satellite, $\bar{\epsilon}$ the over-all value of the infrared emissivity of the satellite, t_e the eclipse time, t_o the orbital period, $\bar{\alpha}$ the mean value of the earth's albedo, \bar{f} the mean integral value of the albedo, and \bar{g} the mean integral value of the earth's infrared radiation. Equation (1) is derived from the consideration that the orbital mean average temperature of the skin of the satellite, \bar{T}_s , can be determined from a balance between the total heat energy absorbed over one orbit and the energy emitted by the satellite during the same orbit, according to the Stefan-Boltzmann law. This equation applies for an isotropic sphere and represents the effective radiation temperature of the skin; for the important special case of two lumped masses, M_s and M_p , it may be used to obtain a convenient reference temperature for the instrument package, as will be shown below.

For an elliptical orbit, the speed of the satellite varies according to Kepler's law, which states that equal areas are swept out in equal times by the radius vector. Therefore, in getting the values of \bar{f} and \bar{g} , time must be taken as the weighting factor. The integration itself is best carried out numerically.

To get the upper limit for \bar{T}_s , one has to consider that, in general, the contribution due to the eclipse time t_e is relatively more important than that due to \bar{f} and \bar{g} . Therefore, it is sufficiently accurate to calculate \bar{f} and \bar{g} for the case where $t_e = 0$ is combined with the largest possible albedo effect. This is the case when the satellite just grazes the earth's shadow at apogee.

Similarly, one can set the lower limit on \bar{T}_s by considering in (1) the longest eclipse time t_e compatible with the given orbital configuration. These two temperature extremes $\bar{T}_{\max,s}$ and $\bar{T}_{\min,s}$ can, for a given orbit and $\bar{\alpha}/\bar{\epsilon}$, be conveniently expressed in terms of an equivalent solar constant S_{eq}

$$T_s = \left(\frac{S_{\text{eq}} \bar{\alpha}}{4\sigma \bar{\epsilon}}\right)^{\frac{1}{4}} \quad (2)$$

For an orbit of 500 nm perigee and 3000 nm apogee, $\bar{T}_{\max,s}$ corresponds to $S_{\text{eq}} = 1.19 S$, and $\bar{T}_{\min,s}$ to $S_{\text{eq}} = 0.917 S$. A value of $\bar{\alpha}/\bar{\epsilon}$ of 0.65

was obtained from calculations based upon the individual surface properties of the skin exterior and was subsequently confirmed by space chamber measurements on several spacecraft models, as will be described later.

For a given S_{eq} and $\bar{\alpha}/\bar{\epsilon}$, the temperature \bar{T}_s can be easily calculated from (2). If this temperature is reached (for example, in the space chamber), it means that the satellite has been exposed to the equivalent "full sunlight" or "maximum eclipse" corresponding to the maximum and the minimum values of S_{eq} , respectively. Thus experimental determination of temperature extremes of all internal components becomes a possibility.

3.4 Thermal Design Considerations for Electronics Package

The information on S_{eq} and the extremes of \bar{T}_s may be used in the design of the electronics package in the following way: in the steady state, and in the absence of heat conduction to the skin, the package will assume the temperature \bar{T}_p defined by the equation

$$Q_p = A_p h \sigma [\bar{T}_p^4 - \bar{T}_s^4] \quad (3)$$

where Q_p is the heat power developed in the package due to the operation of its electronic components and battery charging and h is the overall effective emissivity of the package-skin system. A_p is the surface area of the package.

For a package with a high internal thermal conductivity as a feature of its design, \bar{T}_p will not differ significantly from the operating temperatures of its internal components. The extremes on \bar{T}_p will be obtained from (3). The extreme values of Q_p depend, for a given design of the solar-cell power plant, upon the orientation of the spin axis of the satellite with respect to the sun (a major factor in the output of the solar cells) and upon radiation damage to the solar power plant in space.

The solar plant output has been calculated to be $Q_{p,min} = 7$ watts if the spin axis stays parallel to sun rays for an extended period of time, and $Q_{p,max} = 14$ watts for the initial power with the spin axis perpendicular to the sun's rays.² The minimum power figure took into account a 30 per cent deterioration factor due to the space environment during a two-year period, and also included the effects of shading during the eclipse time. The minimum power figure also considered the elevated temperatures of the active areas of the solar cell plant that result from the parallel orientation of the spin axis with respect to the sun's rays. The higher power figure reflects the fact that, for a spin-stabilized

satellite with the proper orientation of the spin axis, spinning is effective in reducing the solar cell temperatures, with improved conversion efficiency. For thermal tests, a conservative value of 16 watts was used for the maximum power, a value based upon very early estimates of the maximum possible power from the plant.

For a given h , the extremes of the calculated values of Q_P and \bar{T}_s will determine the extremes of \bar{T}_P from (3). The calculated extremes of \bar{T}_P must then fall into the range of temperatures compatible with efficient and reliable operation of all temperature-sensitive package components. The design objectives of maintaining a temperature range of 15°F–90°F on the periphery of the electronics package were the result of an assessment of the reasonable minimum and maximum operating temperatures of the vital components of the package.¹ Initial calculations indicated that these temperature requirements for \bar{T}_P could not be maintained for a fixed h because of the rather drastic changes in S_{eq} and Q_P discussed above. In addition, with respect to \bar{T}_P certain safety margins had to be taken into consideration to account for changes in surface properties of the skin due to the space environment, and to include unavoidable differences between individual satellite models due to processing and assembly. One way of doing this would have been to include the expected variation of $\bar{\alpha}/\bar{\epsilon}$ in the calculation of S_{eq} , with the alternative of simply adding reasonable safety margins to the skin temperature directly.

It was determined that $\bar{\alpha}/\bar{\epsilon} \pm \Delta(\bar{\alpha}/\bar{\epsilon}) = 0.65 \pm 0.1$ was a realistic figure, based on possible variation of the properties of the skin, both initially and after the satellite was subjected for a long time to the space environment. Using the figure of 0.65 for $\bar{\alpha}/\bar{\epsilon}$, \bar{T}_s for a fully sunlit condition is 12°F, and for the maximum eclipse time of 45 minutes, \bar{T}_s is –18°F. In practice, the effect of this variation in $\bar{\alpha}/\bar{\epsilon}$ could be reflected in its influence on package temperatures by applying a safety margin of $\pm 18^\circ\text{F}$ directly to the skin. The $\pm 18^\circ\text{F}$ safety margin is also the figure recommended by NASA from their experience. As will be pointed out later, the calculated values plus 18°F margins were used for space chamber simulation.

3.5 Active Temperature Control System

In the foregoing discussion it was pointed out that the effective emissivity parameter h in (2) would have to be made variable in a suitable way to maintain a range of 15°F–90°F for the electronics package shell. The variable emissivity would also assist in maintaining the shell close to the room temperature objective previously mentioned.

This was accomplished by providing thermostatically controlled "black areas" on surfaces that had to be otherwise insulated to keep the general temperature level of the package higher than the skin reference temperature. The black areas on the surface of the package were obtained by coating with Parson's black lacquer.* Because of the relatively large surface area of the package and the small amount of power available for heating it internally, the whole package exterior was insulated with up to 30 layers of aluminized Mylar, with fiber glass separators.

The amount of exposed black area was controlled by two independently operated, umbrella-type shutters (Fig. 1) that could close very tightly for situations where maximum eclipse and low power input would require a relatively low value of the effective emissivity h . The control element was a bellows filled with n-pentane, designed to be completely open at 75°F and fully closed at 55°F. Because the bellows had to operate in the vacuum environment, a spring arrangement was used to keep the operating fluid at nearly constant pressure. Experimentally, it was verified that the required h range of $0.05 \leq h \leq 0.1$ had been achieved. It must be stated here, however, that the active thermal system designed for the Telstar satellite had to respond primarily to the long-term changes in orbital parameters for purposes of temperature stabilization. For short-term temperature changes (such as those due to a single eclipse), the particular radiative coupling chosen, together with the long time constant of the package with the shutters nearly closed, provided for a temperature response of the package of less than 3°F, as telemetered from the satellite in orbit. It was found experimentally that, should one of the shutters fail, the temperature of the package wall would only slightly exceed the 15°F–90°F range.

3.6 Thermal Design of Satellite Skin

The energy conversion efficiency of solar cells is temperature dependent; the operating efficiency increases as the temperature is reduced. A design objective of approximately 30°F was determined to be a practical average temperature for solar cell operation. This value was based on a compromise between the power required from the solar cell plant, the area on the skin used as cooling areas, and the influence of shell temperature on the package temperature (3). Therefore, the overall temperature level of the skin has to be low. Since the α/ϵ of the

* Parson's black lacquer, distributed by Eppley Laboratories, Newport, R. I.

sapphire-covered solar cell module was about 1.5, additional cooling areas of low absorptivity and high emissivity were dispersed between banks of solar cells.* For the cooling areas, surfaces covered with plasma-jet deposited aluminum oxide with $\alpha/\epsilon = 0.26$ were used. This arrangement resulted in the characteristic checkered appearance of the spacecraft shell, which has an over-all value of $\bar{\alpha}/\bar{\epsilon} = 0.65$ for the entire skin.

In addition to having low absorptivity, the external surface finish must be adherent and stable in space to assure that the cooling effect will be maintained. The surface properties of the 5-mil layer of rough aluminum oxide should be insensitive to change because of abrasion by micrometeoroids in space. The stability of plasma-sprayed aluminum oxide coatings was evaluated in the laboratory, prior to their final selection, by examining their absorptivity and emissivity and by measuring changes in these values with exposure to high vacuum, ultraviolet radiation and electron bombardment. Because the material is a fused inorganic compound, it exhibits high-vacuum stability. Also, its optical properties are more stable than the optical properties of other materials which might have been used for this purpose. The absorptivity of the aluminum oxide surface increased from 0.21 to 0.24 when exposed to ultraviolet radiation equivalent to 8 months in orbit. Thereafter, the absorptivity did not change with further irradiation equivalent to 18 months in orbit. Other tests showed that absorptivity increases from 0.21 to 0.25 after radiation with 100-Kev electrons equivalent to three months in orbit. Additional electron radiation did not cause further change in the absorptivity. The emissivity of the aluminum oxide coating does not change with any of the environmental stresses described above. Therefore, the skin temperature of the satellite should increase slowly with its time in orbit; this will be discussed later in more detail.

A separate investigation¹⁰ was conducted to establish the minimum spin rates for which satellite surface temperatures are radially uniform, so that local surface temperatures are symmetrical with respect to the spin axis. This investigation showed that a spin rate of 3 to 4 rpm is adequate to achieve a radially symmetric temperature distribution. Spinning the satellite, with proper alignment of the spin axis with respect to the sun, reduces the temperatures of the areas in sunlight below those of comparable areas on a nonspinning satellite.

In the above temperature calculations, thin-shell techniques for temperature distribution in the skin have been used. This was again

* The solar cells were covered with sapphire windows to protect them against space hazards. The module was designed to minimize the greenhouse effect due to the presence of the sapphire windows, and to conduct heat efficiently to the skin structure of the satellite.

mainly possible because of the effective separation of the satellite into two lumped masses, that of the skin and that of the package, and through careful elimination of conduction between them. In order to reduce the temperature of areas directly exposed to the solar light, a provision was made for internal radiative heat exchange between hot and cold portions of the skin. Internal radiation has also been found to be very effective in reducing the undesirable temperature differences between the aluminum oxide covered areas of the skin and the areas occupied by the solar cell modules.

The internal surface of the satellite shell and the frame were coated with a white polyurethane paint. Since the finish for the inside of the satellite is not subject to ultraviolet radiation and is less susceptible to electron damage than the external finish, the principal factors to be considered in its selection are high emissivity, vacuum stability and ease of application. The organic finish was chosen in preference to aluminum oxide primarily because it could be applied without the danger of thermally stressing the panels and the satellite frame. The white polyurethane finish has an emissivity of 0.85 and does not change with exposure to vacuum at the temperatures of the satellite shell in orbit.

Methods for calculating local surface temperatures for several orientations of a spinning satellite have been derived.¹¹ In the design stage of the spacecraft, surface temperature distribution was calculated using the above techniques, which take into account the local variation of the $\bar{\alpha}/\bar{\epsilon}$ due to inhomogeneous composition of the individual satellite facet surfaces, internal radiation and orientation of the spin axis with respect to the sun rays.

It can be shown that the appropriate formulas are, for the j th facet, whose normal makes the angle θ_j with the sun rays

$$T_j = T_j \frac{\sqrt{2}}{(1 + \beta_j')^{\frac{1}{2}}} (\cos \theta_j + \beta_j/4)^{\frac{1}{2}} \quad (4)$$

for the case of spin axis being parallel to sun rays, and

$$T_j = T_j \frac{\sqrt{2}}{\pi^{\frac{1}{2}}(1 + \beta)^{\frac{1}{2}}} \left[\cos(90^\circ - \theta_j) + \frac{\pi}{4} \beta_j \right]^{\frac{1}{2}} \quad (5)$$

for spin axis perpendicular to sun rays.

For the intermediate orientations, similar formulas have been developed. In (4) and (5), T_j refers to T as a function of the local values of α_j and ϵ_j . The term β stands for the contribution due to the internal radiation (which depends on the internal emissivity, ϵ_i) and is defined as $\beta_j = \epsilon_i/\bar{\epsilon}_j$. Since for the case of the spin axis being aligned with the

sun rays (4) the effect of the instrument package is to reduce the internal heat transfer the "effective value" of β , β' , is used instead of the full value of β . As a first approximation, β' is proportional to the amount of free area at the equator of the satellite and to β . The results of temperature calculations using (4) and (5) are shown in Table II; the temperatures for 30° and 60° orientations calculated by other equations are also included. For comparison, some telemetered data from orbits 9 and 17 are shown.

The temperatures listed in Table II were intended to be limiting values, so that the power output calculated from the solar cell plant would not be over-optimistic. For the indicated temperatures, a safety margin of 18°F was included to take care of changes in coating characteristics in space, solar cell module thermal impedance and variations in the secondary radiation from the earth. The calculated temperature extremes for the solar cell modules when the satellite spin axis is parallel to the sun are 150°F for the pole nearest the sun and -150°F for the pole away from the sun after a 45-minute eclipse. These limits were used for the design of the solar cell modules and antenna feed components.^{2,4}

In the temperature calculations, the secondary radiation effects were included as average values regardless of satellite altitude and spin axis orientation in relation to the earth, whereas telemetered temperatures include secondary radiation effects for the particular altitude and orien-

TABLE II—LOCAL TEMPERATURE DISTRIBUTION OF SOLAR CELL BANDS* ($^\circ\text{F}$)

Band	Calculated				Telemetry Data from Space			
							Orbit 9	Orbit 17
	Angle Between Spin Axis and Sun Rays							
	0°	30°	60°	90°	90°	90°	90°	
1	156	120	59	27	26	26	19	
2	145	111	77	46	38	38	32	
3	55	46	46	34	36	36	35	
4	†	-94	-29	34	43	43	45	
5			-41	46	30	30	32	
6			-92	27	26	26	29	

* A band is a faceted zone of the skin contained between two planes which are perpendicular to the spin axis of the satellite. The bands are numbered in the table starting at one pole. Bands 1 and 6 are at the poles; bands 3 and 4 are adjacent to the communications antennas.

† Temperatures for bands that do not see the sun directly have not been included in the table.

tation of the satellite at the time the data were taken. In view of these factors, results compare very favorably with predictions.

IV. SATELLITE TESTS IN THE SPACE SIMULATOR

Experimental evaluation of the thermal design of the spacecraft was conducted in a space simulation chamber, with solar radiation provided by carbon arc lamps. The thermal test program had a twofold objective. The first objective was determination of the over-all ratio of solar absorptivity to infrared emissivity of the complete satellite, to verify calculations based upon individual measurements of the satellite's exterior surfaces. Such tests were performed on several satellites with various orientations of the spin axis to the light beam from the solar simulator. With the $\bar{\alpha}/\bar{\epsilon}$ ratio known, the thermal environment for the electronics package can be determined from (2) and (3). The other objective was to simulate extreme orbital conditions, such as full sunlight and maximum eclipse periods, so that the anticipated thermal performance in space could be verified by on-the-ground tests.

4.1 Determination of $\bar{\alpha}/\bar{\epsilon}$ from Simulator Tests

The appendix describes the space simulation facility and presents the method used to calibrate the chamber. The black- and Al_2O_3 -coated satellite experiments determined the average values of solar flux and infrared flux for the case when a real spacecraft was tested in the chamber.

Using these values, four satellite shells were tested in the space chamber under various conditions of illumination to determine the average value of $\bar{\alpha}/\bar{\epsilon}$. These tests were conducted with illumination normal to the spin axis; see Table III. The average $\bar{\alpha}/\bar{\epsilon}$ of the four satellites for illumination normal to the spin axis is 0.702. An experiment was also conducted to determine the variation in \bar{T}_s for spin-axis orientations to the arc lamps of 0° , 30° , 60° and 90° , and showed that \bar{T}_s varied by less than 1.5 per cent for these four orientations.

TABLE III

Satellite Shell	Average $\bar{\alpha}/\bar{\epsilon}$
Mechanical model	0.700
Prototype	0.699
Flyable model no. 1	0.695
Flyable model no. 2	0.716

The $\bar{\alpha}/\bar{\epsilon}$ ratio determined in the space chamber experiments is well within the design tolerance for $\bar{\alpha}/\bar{\epsilon}$ of 0.65 ± 0.1 . Using this median value for $\bar{\alpha}/\bar{\epsilon}$ of 0.65 with the S_{eq} from Section 3.3 ranging from 0.917 to 1.19, the temperature extremes that the satellite skin will experience in its intended orbit will be $\bar{T}_{s,low} = -18^{\circ}\text{F}$ and $\bar{T}_{s,high} = 12^{\circ}\text{F}$. With an 18°F safety margin, limiting mean skin temperatures are $\bar{T}_{s,low} = -36^{\circ}\text{F}$ and $\bar{T}_{s,high} = 30^{\circ}\text{F}$. These limiting temperatures were simulated in the chamber with an arc lamp schedule of 2.93 lamps and 1.57 lamps respectively. The lamp schedule refers to the average number of lamps in operation during a test, where a fractional lamp represents the ratio of its "on" time to total test time. Fig. 8 is a plot of mean spacecraft shell temperatures as a function of the arc lamp schedule for four shells tested in the space chamber.

4.2 Space Simulation Tests

During development, many thermal tests were performed on two thermal models and on the mechanical development model. These models were essentially complete, except that a dummy electronics package with heat dissipation means was used in lieu of actual components in the package. Except for thermal conductivity effects internal

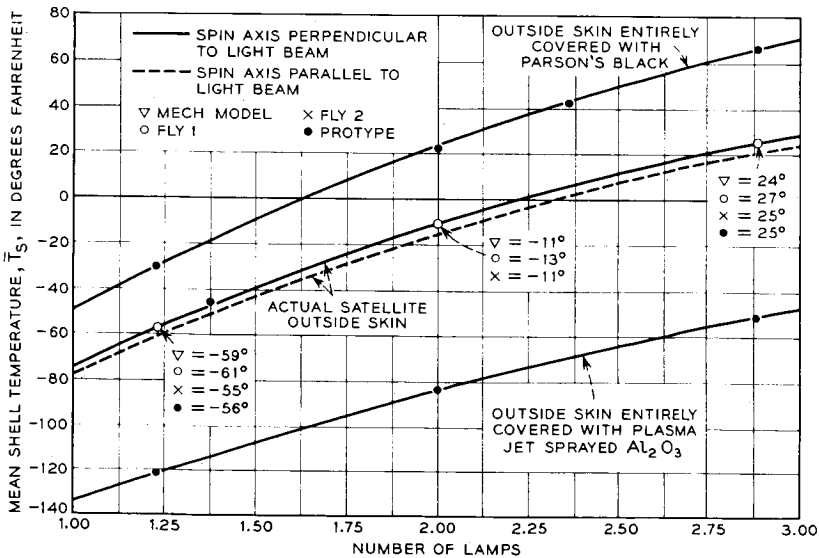


Fig. 8 — Mean shell temperature test results.

to the electronics package, these thermal models duplicated in every respect the thermal behavior of the complete spacecraft in the chamber. These tests were performed to determine the \bar{T}_s of several spacecraft shells, to develop the required degree of emissivity control for the electronics package, to develop support techniques to minimize thermal conduction along the leads from the package to the skin, and to evaluate the operation of the thermal control mechanisms.

In addition, thermal tests were performed on the mechanical development model to evaluate the electronics package temperatures under extreme conditions. The tests listed below were of particular interest in comparing on-the-ground predictions with space performance. The test conditions were:

(a) initial conditions in orbit — maximum power in electronics package (16 watts), full sunlight, $+18^\circ\text{F}$ margin on satellite skin, spin axis perpendicular to solar simulator beam, and

(b) end-of-life conditions (two years) — minimum power in electronics package (7 watts), maximum eclipse, -18°F margin on satellite skin, spin axis perpendicular to solar simulator beam.

These test conditions were more stringent than those predicted for the spacecraft in orbit, for the following reasons:

(a) With the initial highest power from the solar plant dissipated in the electronics package, the satellite skin temperature included the $+18^\circ\text{F}$ safety margin for a full sunlit orbit. Part of this safety margin was for space deterioration effects on the surface coatings, which tend to warm the skin. Based upon measurements of the surface coating deterioration, this condition would not occur until after several months in orbit, at which time the power from the solar plant would be lower.

(b) With the minimum power at the end of two years in space dissipated in the electronics package, the satellite skin temperature was operated with a -18°F safety margin for a fully eclipsed orbit. After two years in orbit, the skin temperature would have been higher than its initial value because of deterioration of the surface coatings.

Nevertheless, these tests were conducted in this manner to be sure that the 15°F to 90°F limits could be met under extreme theoretical conditions. The results of these two extreme tests are given in Table IV along with the anticipated temperatures.

It is interesting to compare the actual package wall temperatures encountered in space with those predicted by the foregoing tests. Fig. 9 is a graph of the package wall temperatures versus time for the satellite's first seven months in orbit. Also included are the eclipse times, which significantly affect package temperatures as well as the power dissipated

TABLE IV

(a) Initial Conditions (Full Sunlight — 16 Watts Maximum Power)	
Measured Package Wall Temperature with +18°F Margin on Skin	Anticipated Package Wall Temperature in Space
87°F	73°F*

(b) End of Life (Maximum Eclipse — 7 Watts Minimum Power)	
Measured Package Wall Temperature with -18°F Margin on Skin	Anticipated Package Wall Temperature in Space
34°F	55°F

* The 18°F margin on the mean skin temperature in (a) is reflected as a 14°F difference in the package wall temperature. In (b), the 21°F temperature difference is a result of the 14°F margin plus a 7°F addition to account for increased absorptivity due to deterioration of surface coatings.

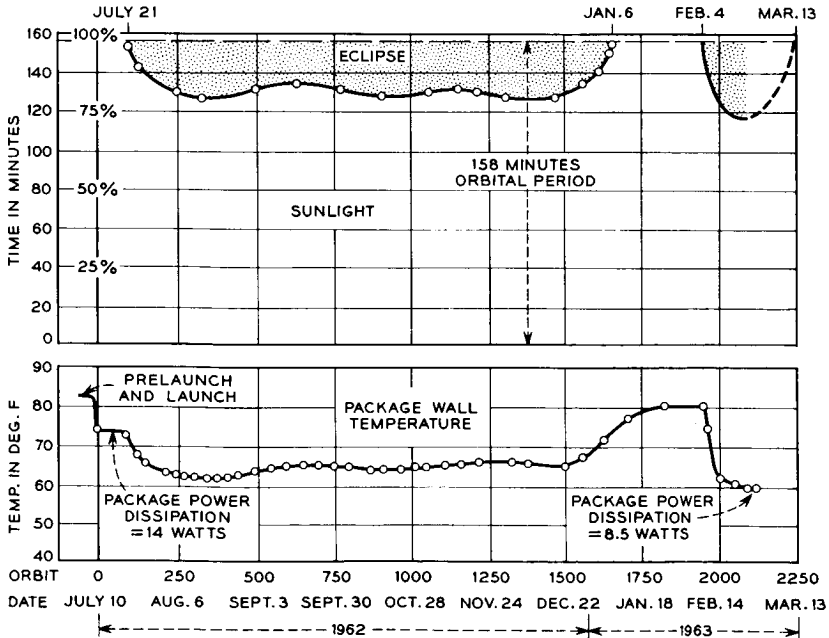


Fig. 9 — Package wall temperature as related to eclipse time.

in the package. The initial temperature in a fully sunlit orbit was 74°F , in comparison to the anticipated 73°F which, of course, had an uncertainty margin of several degrees. At the end of seven and one-half months, the satellite was in the maximum eclipse period of 45 minutes, and the package wall temperature was 60°F with 8.5 watts average orbital power dissipated in the package. At this time the spin axis was nearly normal to the sun. Hence the 60°F temperature encountered in space with 8.5 watts dissipated in the package can be compared to the on-the-ground test figure of 55°F with 7 watts dissipated in the package. The 1.5 watt higher power in space easily accounts for the 5°F higher temperature on the package. It must be emphasized again that these package wall temperatures provide the environment for the electronic components and are not the actual temperatures of the components themselves, which run slightly warmer.¹

A few over-all observations should be made regarding the package wall temperature in space, shown in Fig. 9. Just prior to launch, the package temperature was 83°F ; within nine orbits it dropped to 74°F , where it remained stable for two weeks while the satellite was in a fully sunlit orbit. It will be noted that the variation in package temperature followed very closely the percentage of time that the satellite was in the sun. In January, 1963, the satellite was again in a fully sunlit orbit and the package temperature was about 6°F warmer than in July, 1962. This 6°F change in electronics package temperature can be accounted for by the cumulative effects of the three factors outlined below; figures in parentheses are estimated effects of change on package temperature:

(a) In January the solar constant is 7 per cent higher than it is in July ($+6^{\circ}\text{F}$),

(b) The absorptivity of the aluminum oxide coating on the satellite skin is presumed to have increased because of ultraviolet and particle radiation effects ($+5^{\circ}\text{F}$), and

(c) The power dissipated in the electronics package was decreased from 14 watts in July to 11 watts in January (-5°F).

Had the satellite's spin axis precessed from being reasonably perpendicular to the sun rays, there would have been a minimum electronics package wall temperature. Based upon solar simulator tests, the lowest package temperature would be reached with the spin axis parallel to the sun at the end of a two-year life in orbit. In the simulated test, the measured package wall temperature was 14°F with the -18°F safety margin on the skin and the 7 watts expected minimum power in the package. For the reasons outlined previously, the estimated 14°F seems to be unrealistically low: the expected temperature would be 21°F higher, or 35°F .

During the seven months the satellite has been in orbit, the spin axis has remained within 10° of being normal to the sun rays.¹² Hence, no space confirmation of this minimum figure has been possible.

V. CONCLUSIONS

The important features of the Telstar spacecraft structural and thermal design have been presented. In addition, the details of the comprehensive development and environmental test programs have been reviewed.

All mechanical and thermal objectives were achieved, as confirmed by several spacecraft having passed the rigorous environmental tests and the satellite's seven-month performance in space at the time of writing.

The over-all structure and method of support for the electronics package have isolated the vital electronics components from the rigors of launch. Other components, associated with the shell structure, have been designed and proven to withstand qualification level testing.

The active temperature control system has provided a near room temperature environment for the electronic components. Telemetered data from the Telstar satellite have shown that the electronics package wall temperature (component environment) has been maintained between 60°F and 80°F during seven months in orbit. Conditions during this period included fully sunlit orbits, maximum 45-minute eclipse orbits, variation of 7 per cent in the solar constant, and a variable package power of 14 watts to 8.5 watts. When the satellite's spin axis has been normal to the sun, the solar cell temperatures have been maintained close to the 30°F objective.

VI. ACKNOWLEDGMENTS

The writers are indebted to L. Rongved and J. W. West, whose advice, valuable ideas, and over-all guidance contributed so much to the success of the spacecraft structural and thermal design.

APPENDIX

Description and Calibration of Space Simulator

A.1 Description

The space simulation facility shown in Figs. 10 and 11 consists of a vacuum chamber with an operating pressure in the low 10^{-6} torr range;

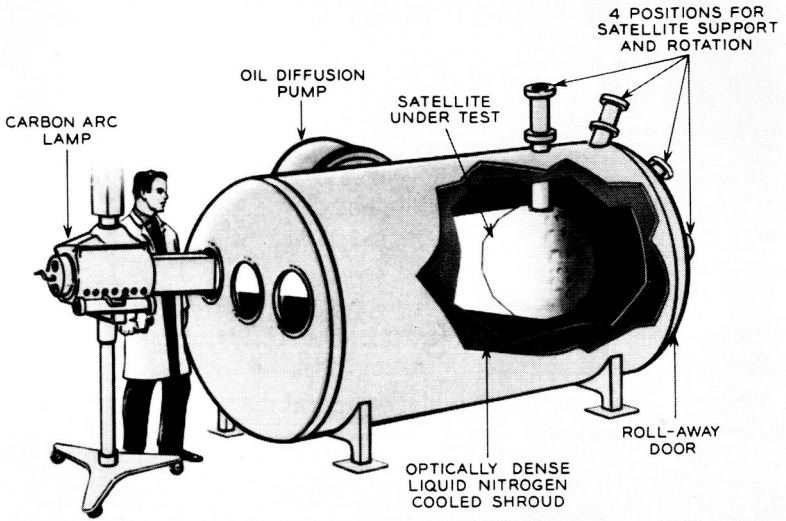


Fig. 10 — Space simulation test facility.

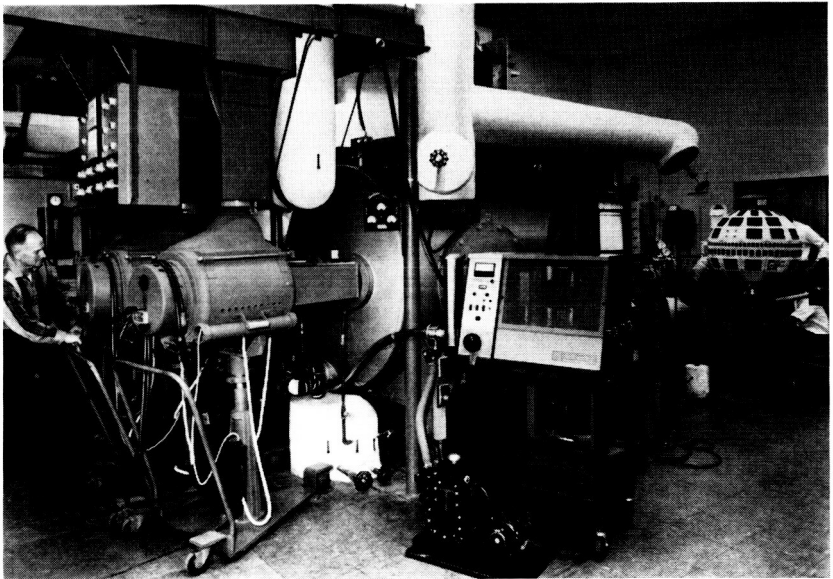


Fig. 11 — Space simulation test facility, showing three carbon arc lamps in place and spacecraft being prepared for test.

a high-absorptivity, liquid nitrogen cooled shroud surrounding the work space; and carbon arc lamps to provide simulated solar energy. The useful working volume in the interior of the chamber is approximately 4.5 feet in diameter by 7 feet long. The solar simulator arc lamps illuminate the spacecraft through three glass ports at the rear of the chamber. Four support positions are provided on the chamber, to permit testing of the satellite with the spin axis at angles of 0° , 30° , 60° and 90° , with respect to the symmetry axis of the chamber.

During the tests, the spacecraft was suspended on a hollow rotating shaft extending into the chamber through a vacuum-tight seal. All electrical leads and instrument connections were brought through the shaft to vacuum-tight feedthroughs at the shaft end. During a test, the spacecraft was rotated about its spin axis; the direction of rotation was reversed about every six revolutions. All external wire connections were installed with enough slack to allow the wires to twist around themselves during rotation, thereby eliminating the need for slip-rings. The rate of rotation was sufficient to avoid any noticeable temperature fluctuations on the skin as a particular portion of the surface rotated in and out of the beam. The point of reversal was staggered during each cycle to eliminate nonuniform illumination of the surface. The test vehicle was insulated from the shaft to minimize conductive heat loss through the shaft.

The radiation from each arc lamp was collected and focused by four glass lenses, and the intensity of each beam was roughly fixed by adjusting the relative positions of these lenses. Each arc emits over 1300 BTU/hr of simulated solar radiation. No attempt was made to collimate the radiation from the lamps, since lack of collimation has a negligible effect on the determination of the $\bar{\alpha}/\bar{\epsilon}$ ratio for an isotropic spherical spacecraft.

For test purposes, the beam cones of the three arcs were adjusted to extend about two inches past the spacecraft cross section, so that the nonuniform beam edge did not influence the tests. The intensity was found to change with time because of variations in supply voltage, differences in electrodes, etc. However, it was possible to compensate for these intensity changes, without appreciably affecting other characteristics of the radiation, by making small adjustments in the spacing between the positive and negative carbons. This was found to be sufficient to control the intensity variations encountered during any run. Solar cells, which are described below, were suspended in the beam inside the chamber to act as intensity monitors for the arc lamp radiation. The electrode spacing was manually trimmed to maintain predetermined short-circuit current outputs on the solar cell monitors.

In all the tests, the intensity of the individual arc lamps was kept constant, and changes in the time-averaged intensity were accomplished by turning the lamps on and off in a suitably scheduled manner. Each arc lamp could be operated for over an hour before its electrodes were consumed. It was a relatively simple matter at this point to remove the spent lamp and replace it with a freshly carboned one.

Three 1×2 cm solar cells were suspended in the chamber in front of the spacecraft and were used as arc intensity monitors. The short-circuit current from these cells was calibrated against the intensity of the arc lamps and provided a reference for carbon electrode adjustments. During a test, the short-circuit current from banks of solar cells on the spacecraft surface was also recorded. This provided an additional check on the control of the over-all intensity of arc radiation, although these cells were not specifically calibrated for that purpose. While the short-circuit current from the spacecraft solar plant was not used as a standard for adjusting the arc lamp intensity, it was useful in observing changes in the characteristics of the individual solar cell strings.

The spectral characteristics of the radiation from the carbon arc lamp match quite closely the spectrum of the sun's radiation outside the earth's atmosphere (Johnson curve).¹³ The glass lenses in the facility prevent all radiation below 0.35 micron from entering the chamber; however, this small loss in the ultraviolet region does not have a significant effect on the thermal measurements discussed here.

A.2 Arc Lamp Calibration

The arc lamps were positioned to face the center of the test region and were equidistant from it. The centers of the arc beams were all projected along the same horizontal plane, and the areas illuminated by each arc were equal.

The radiation from the arc lamps in the region near the specimen acts as if it were emitted by a point source: i.e., the relationship between intensity and distance is closely represented by an inverse square function. When the power density at the location of the center of the satellite is set equal to some value, I , the average power density on the surface of the spherical satellite from a collimated source also has an intensity I .¹⁶

Each arc lamp was adjusted to give approximately $\frac{1}{3} S$ at the center of the satellite, where S is the solar constant. This was found to provide sufficient radiative input to the test vehicle to produce the maximum energy condition — i.e., a fully sunlit orbit plus appropriate margins. The lamps were then placed in position, and, with the chamber at am-

bient conditions, the three monitoring solar cells were illuminated by the lamps and their output was compared to a calibrated Eppley pyrheliometer at the point corresponding to the center of the test specimen.

A.3 Calibration of Space Simulator

A.3.1 Thermal Balance Equation

The total net power stored in a test specimen in the space simulation chamber can be described by a thermal balance equation of the form

$$Q_T = Q_S + Q_R + Q_{IR} - Q_E \quad (6)$$

where the first three terms on the right represent power absorbed by the specimen from, respectively, the simulated solar source, simulated solar power reflected from the surroundings, and infrared power from the surroundings. The last term in (6) describes the power radiated by the test specimen. Here, we have assumed that all thermal energy exchange is by radiation, and that there is no heat dissipation within the specimen.

At thermal equilibrium, (6) can be set equal to zero and rewritten as:

$$\bar{\alpha}A_1 I + \bar{\rho}\bar{\alpha}A_2 I + \bar{\alpha}'A_1 I_w - \bar{\epsilon}\sigma A_2 \bar{T}_s^4 = 0 \quad (7)$$

where

$\bar{\alpha}$ = average absorptivity of specimen to carbon arc radiation

A_1 = cross-sectional area of specimen

I = time-averaged intensity of carbon arc radiation

$\bar{\rho}$ = fraction of I received by the specimen by reflection from the surroundings, averaged over the surface of the specimen

A_2 = surface area of specimen; for a spherical specimen, $A_2 = 4A_1$

$\bar{\alpha}'$ = average absorptivity of specimen for radiation emitted and reflected by the surroundings in the infrared region

σ = Stefan-Boltzmann constant

I_w = intensity of total equivalent collimated infrared flux emitted and reflected by the surroundings

$\bar{\epsilon}$ = average emissivity of the specimen, and

\bar{T}_s = average temperature of the specimen.

Now, making the simplifying assumption that $\bar{\alpha}' = \bar{\epsilon}$ and substituting the appropriate area factors for a spherical specimen, (7), after a slight rearrangement, becomes

$$\frac{\bar{\alpha}}{\bar{\epsilon}} = \frac{4\sigma\bar{T}_s^4 - I_w}{I(1 + 4\bar{\rho})} \quad (8)$$

A.3.2 Determination of Total Energy Flux in Chamber

The total energy that a satellite receives in the chamber at a particular lamp intensity has been determined in a test on a "black satellite." The black satellite is a dummy satellite shell of the same dimensions as the Telstar satellite, but covered on the entire exterior with Parson's black lacquer. This paint has an absorptivity and emissivity both approximately equal to 0.98. In the center of the hollow black satellite, a small ball was suspended with nonconducting supports and instrumented with thermocouples. The ball and the interior of the black satellite were also painted black. The steady-state temperature that this ball assumes may be shown mathematically to be the mean shell temperature of the black satellite.

The arc lamp energy reflected from the walls with the black and other satellites in the chamber was measured with a calibrated solar cell. The average reflected flux $\bar{\rho}$ with the black satellite was 0.003. Similar measurements were carried out with an actual satellite installed in the chamber, and $\bar{\rho}$ was determined to be 0.007.

The black satellite was installed in the chamber and the test conducted with the walls at liquid nitrogen temperature and the pressure in the 10^{-6} torr range. The arc lamps were turned on, and the equilibrium temperature of the black satellite was recorded at three different lamp intensities, I . Table V gives the results of these tests. The quantity q_c , which represents the total collimated intensity of radiation incident

TABLE V—CALIBRATION OF ENVIRONMENTAL CHAMBER
USING PARSON'S BLACK COATED SPHERE

I BTU/hr-ft ²	\bar{T}_S °R	$\bar{\alpha}/\bar{\epsilon}$	I_w BTU/hr-ft ²	q_c BTU/hr-ft ²
443	526	1	83	530
307	482	1	64	374
189	429	1	44	235
0	215	1	15	15

TABLE VI—DETERMINATION OF $\bar{\alpha}/\bar{\epsilon}$ FOR A *Telstar*
SATELLITE SKIN

I BTU/hr-ft ²	q_c BTU/hr-ft ²	I_w BTU/hr-ft ²	\bar{T}_S °R	$\bar{\alpha}/\bar{\epsilon}$
443	529	73	486	0.68
307	372	56	448	0.70
189	234	39	399	0.70

on the surface of the test specimen, has been computed from the relationship

$$q_c = I(1 + 4\bar{p}) + I_w \quad (9)$$

where the first term on the right is the radiation from the arc lamps (direct plus reflected), and the second term is the thermal infrared radiation.

The quantity q_c was also determined in a similar manner in a test on a jet-sprayed aluminum oxide (Al_2O_3) covered satellite with known α/ϵ ratio. The values of q_c for both tests showed good agreement.

Table VI gives an example of the calculation of $\bar{\alpha}/\bar{\epsilon}$ for one of the actual spacecraft shells measured in the environmental chamber. The temperature \bar{T}_s was determined with a black ball centrally located in the interior of the spacecraft, as in the previous cases. The interior surface of the skin had a high-emissivity finish and no electronics package was used. The $\bar{\alpha}/\bar{\epsilon}$ ratio in the table was determined from (8). With this ratio known, it is now possible to simulate the extreme orbital conditions by adjusting the time-averaged lamp intensity to produce the calculated mean shell temperature from (2).

REFERENCES

1. Shennum, R. H., and Haury, P. T., A General Description of the *Telstar* Satellite, B.S.T.J., this issue, p. 801.
2. Smith, K. D., Gummel, H. K., Bode, J. D., Cuttriss, D. B., Nielsen, R. J., and Rosenzweig, W., The Solar Cells and Their Mounting, B.S.T.J., this issue, Part 3.
3. Yu, E. Y., Spin Decay, Spin Precession Damping, and Spin-Axis Drift of the *Telstar* Satellite, to be published.
4. Bangert, J. T., Engelbrecht, R. S., Harkless, E. T., Sperry, R. V., and Walsh, E. J., The Spacecraft Antennas, B.S.T.J., this issue, p. 869.
5. Delchamps, T. B., Jonasson, G. C., and Swift, R. A., The Spacecraft Test and Evaluation Program, B.S.T.J., this issue, p. 1007.
6. Heller, G., Thermal Control of the Explorer Satellites, ARS Journal, **30**, Apr., 1960, pp. 344-352.
7. Hanel, R. A., Thermostatic Temperature Control of Satellites and Space Vehicles, ARS Journal, **29**, May, 1959, pp. 358-361.
8. Acker, R. M., Lipkis, R. P., and Vehrencamp, J. E., Temperature Control System for the Atlas Able-4 Lunar Satellite, ASME Paper No. 60-AV-46, June, 1960.
9. Hrycak, P., Effects of Secondary Radiation on an Orbiting Satellite, ARS Journal, **32**, Aug., 1962, pp. 1294-1295.
10. Hrycak, P., Temperature Distribution in a Spinning Space Vehicle, AIAA Journal, **1**, Jan., 1963, pp. 96-99.
11. Hrycak, P., Calculation of Satellite Surface Temperature Distribution, to be published.
12. Hutchison, P. T., and Swift, R. A., Results of the *Telstar* Satellite Space Experiments, B.S.T.J., this issue, Part 2.
13. Hrycak, P., Unger, B. A., and Wittenberg, A. M., Thermal Testing of the *Telstar* Satellite, Proc. Inst. Environmental Sci., 1963, pp. 477-484.